Supplementary Information

Ultrafast and reproducible quantitative analysis of bacterial chemotaxis by microfluidic cell counting and imaging

Chenwei Xiong[a], Bing Fu[a#]

[a]Department of Biomedical Engineering, City University of Hong Kong, Hong Kong, Hong Kong SAR, China

#Address correspondence to Bing Fu: bingfu@cityu.edu.hk

1. Microfluidic Device Design, Fabrication, and Configuration

1.1 Device design

The microfluidic devices were designed using AutoCAD software. The design was printed as a high-resolution plastic film mask by a commercial supplier (Supplementary Figure 1a). The offline device layout consists of a single straight rectangular microchannel with a length of 10 mm and a cross-section of 100 μm (width) × 40 μm (height). The channel terminates in two circular access ports: an inlet for sample injection and an outlet for waste collection (Supplementary Figure 1b). To evaluate geometric tolerance, additional devices were designed with channel heights of 20, 40, and 80 μm at a fixed width of 100 μm, and with channel widths of 50, 100, and 200 μm at a fixed height of 40 μm. The channel length, port positions, and central imaging region were kept identical among all geometric variants.

The integrated device contains a straight rectangular microchannel with a length of 10 mm, a width of 200 μm, and a height of 40 μm (Figure 5a). After PDMS curing and demolding, the reservoir (2 mm × 5 mm) is created directly by cutting through the cured PDMS slab with a blade, exposing the glass substrate at the bottom and forming an open well that holds 50 μL of bacterial suspension. One end of the microchannel opens into the reservoir. The other end is closed with no outlet port, making the microchannel dead ended. The chemo-effector gradient occurs at the reservoir-channel interface, and the imaging regions of interest (ROIs) were placed 67, 100, and 133 μm downstream of the interface. In this design, the channel serves as both the chemotaxis migration region and the *in situ* counting region, and all experiments are performed under static, flow-free conditions.

1.2 Fabrication

The microfluidic devices were fabricated using standard soft lithography and replica molding techniques. A 3-inch silicon wafer was used as the substrate for master mold fabrication. The wafer was first cleaned and dehydrated on a hot plate. To do the photoresist spin-coating, a negative photoresist (SU-8 3025, MicroChem, USA) was spin-coated onto the silicon wafer to a target thickness of 40 μm. Then the coated wafer was pre-baked at 95 °C for 20 min to remove solvent from the photoresist layer. When doing the UV exposure, the photomask bearing the channel design was placed over the wafer, and the assembly was exposed to UV light. In the

case of negative-tone SU-8 photoresist, only the regions corresponding to the channel pattern (exposed to UV) undergo cross-linking and become cured, while the masked regions remain uncured. After that, the post-exposure baking was required. The exposed wafer was post-baked at 95 °C for 8 min to complete the cross-linking reaction. Finally, development was conducted. The wafer was immersed in SU-8 developer solution, which dissolved the uncured (unexposed) regions of the photoresist, leaving behind the patterned channel structures on the wafer surface. The resulting silicon master mold was then dried and stored in a Petri dish for subsequent PDMS molding.

To prepare the Polydimethylsiloxane (PDMS) slab, prepolymer (Sylgard 184, Dow Corning) was mixed thoroughly with its curing agent at a weight ratio of 10:1. The PDMS mixture was then poured over the SU-8 master mold placed in a Petri dish. To remove air bubbles trapped in the PDMS, the assembly was placed in a vacuum desiccator and degassed until all bubbles were eliminated. The PDMS was cured at 60 °C overnight to allow complete polymerization of the elastomer. After curing, the PDMS slab was carefully peeled off from the master mold. The microchannel pattern was thereby replicated as negative relief features on the PDMS surface. The cured PDMS slab was cut into individual device pieces. For the offline device, inlet and outlet ports were created using a hole puncher. The access holes should match the outer diameter of the tubing to be used for fluidic connections.

After fabricating the PDMS slab with a microchannel pattern, the PDMS replica (with channel side facing up) and a cleaned glass slide were treated with air plasma to activate their surfaces. Plasma treatment generates reactive silanol (Si–OH) groups on both surfaces, enabling irreversible bonding. The plasma-treated PDMS and glass slide were brought into conformal contact and pressed gently to form an irreversible seal. The bonded device was then placed on a hotplate at ~70 °C for an hour to strengthen the bonding.

1.3 Device operation

For the offline mode, bacterial suspensions are loaded into a syringe and driven through the channel from inlet to outlet at controlled flow rates (typically 2–10 μL/h) using a syringe pump. The device is then placed on an inverted microscope stage, and the region of interest (ROI) is moved to the center of the channel. Continuous images are captured with a water immersion 60× objective (pixel size = 183 nm) and the number of bacteria passing the counting line is counted using a customized MATLAB algorithm.

For the integrated mode, the chemotaxis-assay operates entirely under static, flow-free conditions. The microchannel is pre-filled with either chemotaxis buffer or chemo-effector solution using a pipette. The open end of the channel is immersed in 50-μL bacterial suspension loaded in the reservoir (2 mm × 5 mm) (Figure 5a). The assembled device is placed on an inverted microscope stage, and time-lapse bright-field transmission images with 5-min internal are acquired for 60 min using a water immersion 60× objective, with a fixed ROI positioned 100 μm downstream the reservoir–channel interface. For each time-lapse image, the number of bacteria within the ROI is counted using the Cell Counter function in ImageJ. In each experimental condition (chemo-effector or buffer control), these counts were plotted as a

function of time to obtain the bacteria accumulation. To quantify the overall bacteria accumulation up to a given time point, the area under curve (AUC) was calculated. To quantitatively evaluate chemotaxis, the change ratio of the area under the curve (AUC) relative to the respective buffer control was calculated at various cumulative time points (10, 20, 30, 40, 50, and 60 min):

$$Change\ ratio = \frac{AUC_{chemo-effector} - AUC_{buffer}}{AUC_{buffer}}$$

where $AUC_{chemo-effector}$ is the AUC for the chemo-attractant condition and AUC_{buffer} is that for the corresponding buffer control. This ratio quantifies the relative attraction or repulsion in bacterial accumulation induced by the chemo-effector gradient over time.

2. MATLAB package for cell counting in offline device

2.1 Structure and Module Descriptions

A custom MATLAB code package was developed to perform automated cell detection in the offline microfluidic counter. For each frame, every 2×2 pixel tile is compared with the background. A tile is marked active if the absolute intensity difference is above a threshold. Active tiles are dilated and clustered by DBSCAN to be recognized as bacteria. Bacteria are tracked across frames: the function matchpairs in trackClusters.m is used to link bacteria within 150 pixels in consecutive frames. Each tracked bacterium receives a unique ID. A bacterium is counted once when its centroid crosses the counting line in the center of the FOV. The package provides a GUI for interactive parameter tuning, consisting of six interdependent functional modules and one main entry script.

Main entry script:

cell_detection_GUI.m: This main script initializes the interactive GUI, manages video loading, and frame navigation. It orchestrates all sub-functions and handles user interactions, including threshold adjustments and start/stop.

Functional modules:

computeTileBackground.m: This preprocessing module extracts the first N frames (default N = 50) to compute a tile-wise baseline intensity map. This static background is used as a reference for foreground-background separation.

detectActiveTiles.m: The detection module divides each frame into non-overlapping square tiles (default size = 6 × 6 pixels). For each tile, it calculates the ratio of the current summed intensity to the precomputed background sum. Tiles with a ratio outside the tolerance band are marked as “active”. A morphological dilation is then applied to merge adjacent active tiles.

clusterTiles.m: The spatial clustering module groups active tiles into distinct cell-sized clusters using a DBSCAN-like approach. The clustering radius is determined by the parameter of cluster_distance_threshold. Each cluster’s centroid and its corresponding index are computed and stored.

trackClusters.m: The tracking and counting module implements a linear motion-prediction association algorithm across consecutive frames. It matches clusters from the previous frame to the current frame using a global nearest-neighbour search constrained by a spatial distance_threshold. Trajectories are updated for each matched cluster. When the trajectory of a cluster crosses a predefined exit_zone (near the bottom of the field of view), the bacterium is counted, and its unique ID is added to an all_counted_ids.

visualizeTiles.m: The visualization module overlays active tile boundaries, cluster centroids, the counting exit line, and real-time statistics onto the raw video frame for intuitive visual inspection.

2.2 Operating instructions

2.2.1 Click “Load Video” to select an AVI file.

2.2.2 Use “Previous Frame” / “Next Frame” to manually browse the video.

2.2.3 Adjust “Set Intensity Threshold” or “Set Cluster Distance Threshold” if the default parameters fail to clearly distinguish cells from background noise.

2.2.4 Click “Run” to start the automatic detection and counting loop. The results (active tiles, clusters, and cumulative count) are updated in real-time on the display axis.

2.2.5 Click “Stop” to pause the process or “Quit” to close the interface and release memory.

2.3 Data availability and online repository

The complete source code package has been deposited in a public GitHub repository: github.com/spururs a/Cell-detection-with-flow

3. ImageJ-based counting and single-cell trajectory analysis for the integrated device

3.1 ROI counting using ImageJ Cell Counter

Bacterial counts within each ROI were obtained directly using the ImageJ Cell Counter plugin. When necessary, background subtraction and contrast adjustment were applied only to aid visual identification.

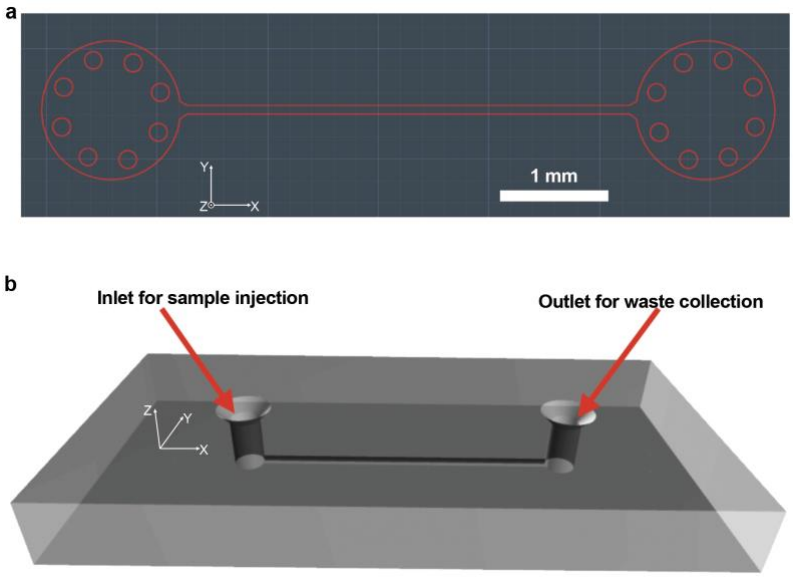
3.2 Single-cell segmentation and tracking

Single-cell trajectories in the integrated device were reconstructed using TrackMate in ImageJ[1], after segmentation by CellposeSAM[2]. Time-lapse image sequences were first imported into ImageJ. CellposeSAM was used to generate binary masks of individual bacteria in each frame, which were then passed to TrackMate for object detection and tracking. The linear assignment problem (LAP) tracker in TrackMate was used to link detections across frames into single-cell trajectories.

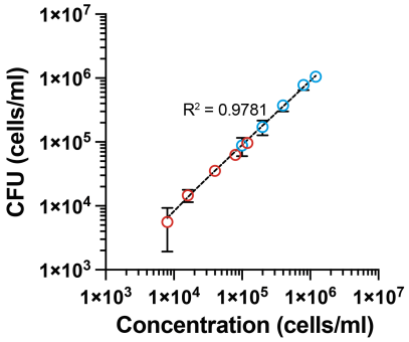
3.3 Chemotaxis index

For each track, the chemotaxis index (CI) was defined as the net displacement projected onto the gradient direction divided by the total accumulated path length. A positive CI indicates net

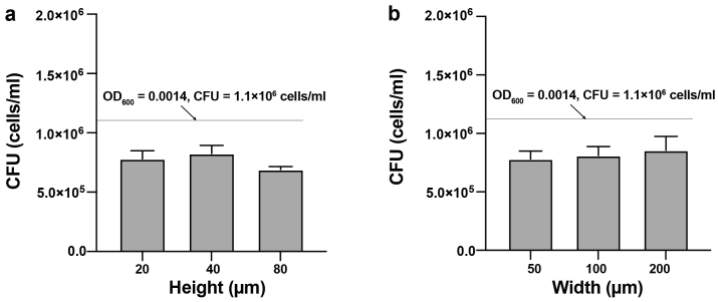
migration toward the gradient, whereas a negative CI indicates migration in the opposite direction.



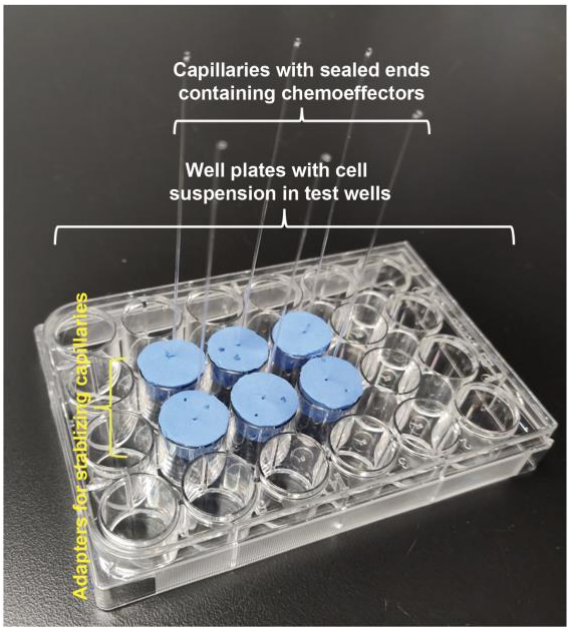
Supplementary Figure 1. Microfluidic counter device **(a)** schematic and **(b)** design.



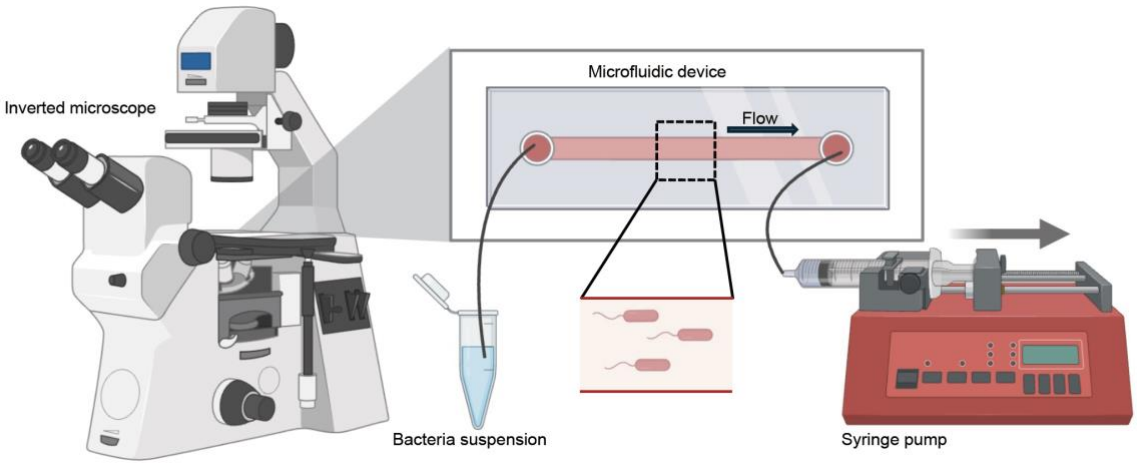
Supplementary Figure 2. Linearity assessment at a broader concentration range between OD_{600} concentration value and CFU value calculated from counts. The red circles represent the condition under low flow rate of 6 µL/h and the blue circles represent the condition under high flow rate of 90 µL/h.



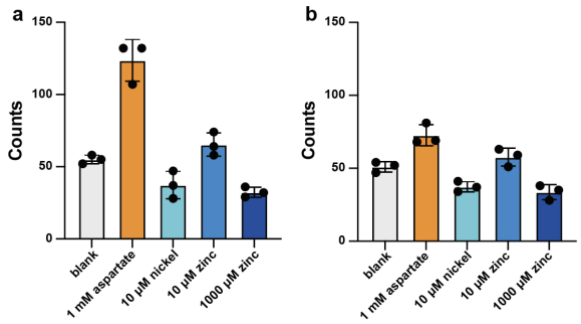
Supplementary Figure 3. Influence of microchannel geometric dimensions on CFU concentration readouts. **(a)** CFU readouts when altering microchannel heights (20, 40, and 80 µm) with a fixed width of 100 µm. **(b)** CFU readouts when altering microchannel width (50, 100, and 200 µm) with a fixed height of 40 µm.



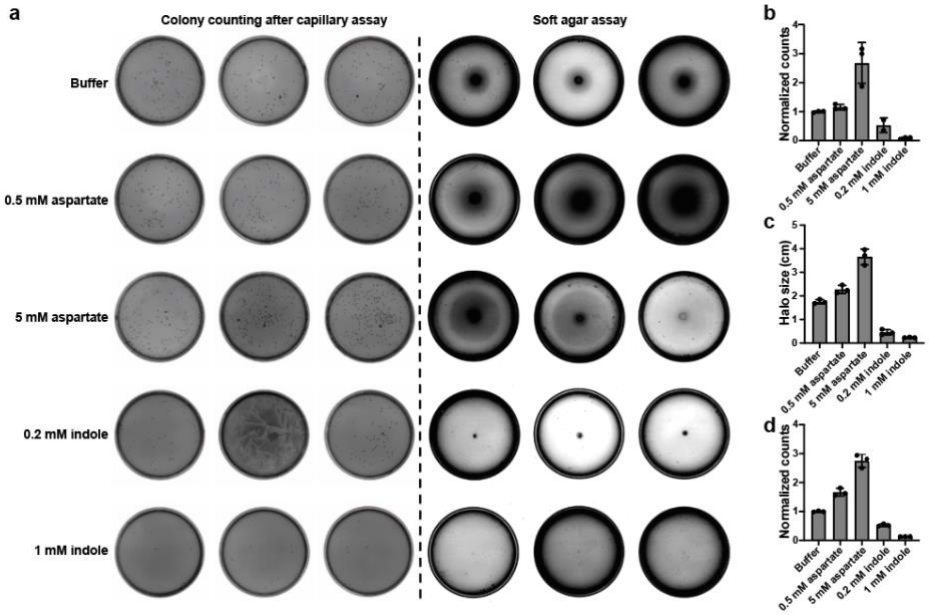
Supplementary Figure 4. Capillary assay setup consisting of three components: capillaries with sealed ends containing chemo-attractants/repellents, well plates with cell suspension in test wells, and adaptors for stabilizing capillaries.



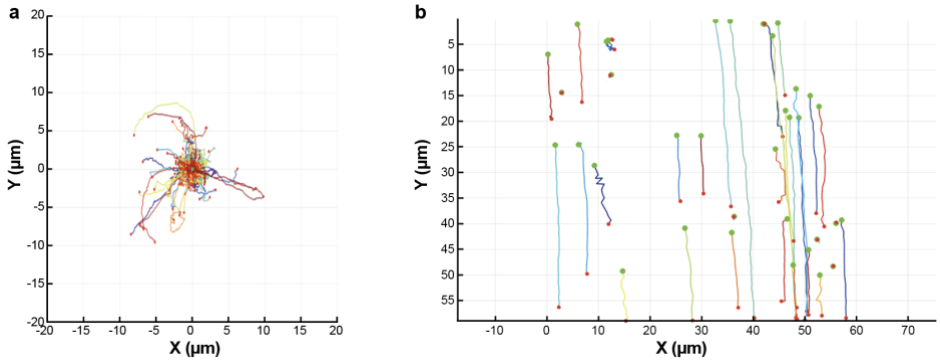
Supplementary Figure 5. Schematic illustration of the offline microfluidic counter setup. The platform consists of a microfluidic device placed on an inverted microscope stage, a tube containing bacterial suspension, and a syringe pump. The syringe pump operates in withdrawal mode to precisely regulate the hydrodynamic flow rate within the microchannel, enabling real-time visualization of bacteria under the flow.



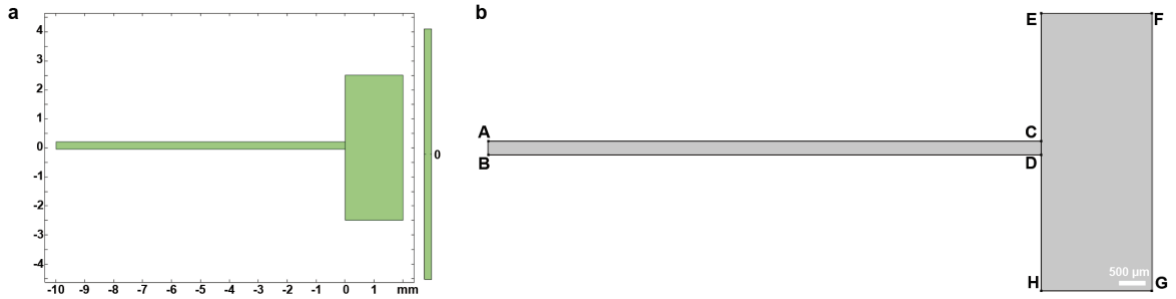
Supplementary Figure 6. Absolute bacterial counts entering the capillaries under various chemical stimuli, including blank buffer, aspartate (1 mM), nickel (10 μM), low-concentration zinc (10 μM), and high-concentration zinc (1000 μM), for **(a)** WT and **(b)** chemoreceptor-deficient (Δ*tar*) *E. coli* strains.



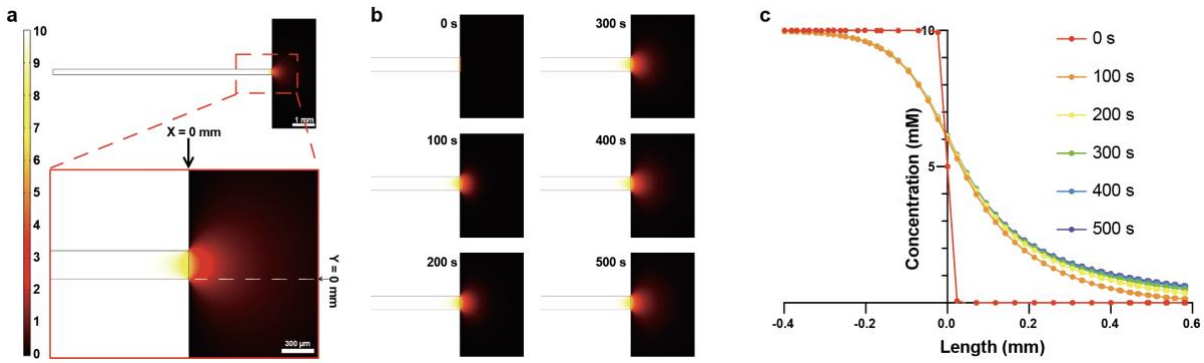
Supplementary Figure 7. Comparison of chemotactic assay heterogeneity among the conventional colony counting method, soft agar assay, and our separated microfluidic device. **(a)** Agar plate pictures of colony counting after capillary assay and soft agar assay. The three plates in each group are three replicates. **(b)** Normalized bacteria counts under different conditions obtained from colony counting after capillary assay. (**c**) Halo size under different conditions obtained from soft agar assay. **(d)** Normalized bacteria counts under different conditions obtained from microfluidic counting after capillary assay.



Supplementary Figure 8. Bacterial swimming trajectories in the integrated device. **(a)** Trajectories of *E. coli* cells recorded within the microchannel in the absence of bulk fluid flow (extracted from Supplementary Movie 2). **(b)** Trajectories of *E. coli* cells under a directional fluid flow (extracted from Supplementary Movie 3).

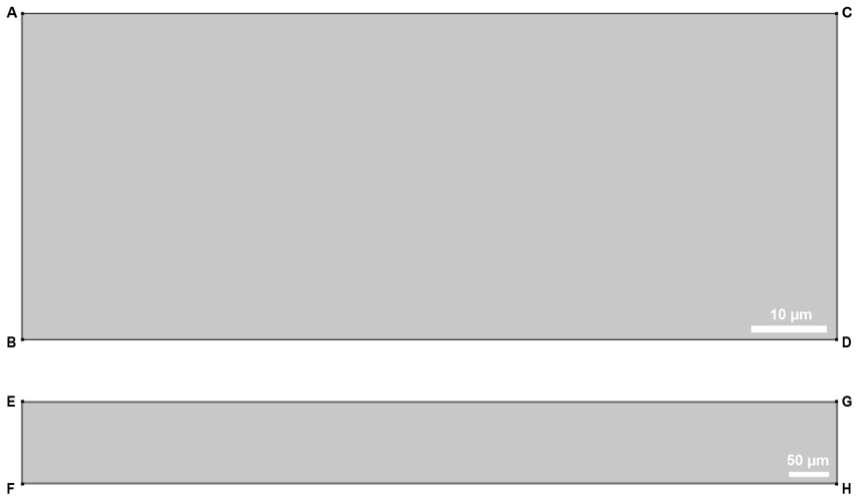


Supplementary Figure 9. **(a)** COMSOL numerical simulation of the flow velocity on the microchannel and reservoir domain in the integrated device. **(b)** Schematic illustration of the 2D computational domain for the chemo-effector concentration gradient at the microchannel-reservoir interface. Scale bar: 500 µm. The physical conditions for each boundary are detailed in Supplementary Table 2.



Supplementary Figure 10. COMSOL numerical simulation of the chemo-effector concentration gradient at the microchannel-reservoir interface in the integrated device. **(a)** The simulation depicts the concentration profile between a 10-mm microchannel (width: 250 µm)

and a reservoir filled with buffer medium (scale bar: 500 μm). The inset shows a magnified view of the microchannel-reservoir interface (scale bar: 200 μm), clearly visualizing the hemispherical diffusion front and the concentration gradient as the aspartate diffuses from the microchannel into the reservoir. **(b)** The time evolution of concentration gradient establishment at the interface between the microchannel and reservoir. **(c)** Concentration profile along the Y = 0 from 0 ~ 500 s.



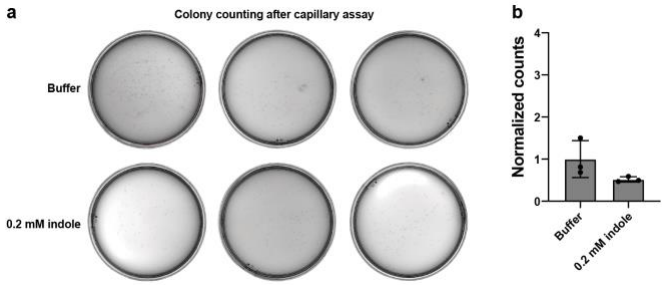
Supplementary Figure 11. Schematic illustration of the 2D computational domain for the velocity profiles in the integrated device. The upper domain is modelled for the vertical cross-section (scale bar: 10 μm), and the bottom domain is modelled for the horizontal view (scale bar: 50 μm). The physical conditions for each boundary are detailed in Supplementary Table 1.

Supplementary Table 1. Boundary conditions for the 2D computational domain in Supplementary Figure 11.

Boundary	**Length**	**Poisson**	**Nernst-Planck**
AC, BD	100 μm	zero charge	insulation
AB, CD	40 μm	zero charge	insulation
EG, FH	1000 μm	zero charge	insulation
EF	100 μm	zero charge	insulation (inlet)
HG	100 μm	zero charge	insulation (outlet)
surface in ACDB		zero charge	initial value (0 mM)
surface in EFHG		zero charge	initial value (0 mM)

Supplementary Table 2. Boundary conditions for the 2D computational domain in Supplementary Figure 9.

Boundary	**Length**	**Poisson**	**Nernst-Planck**
AB	0.25 mm	zero charge	constant concentration (10 mM)
AC, BD	10 mm	zero charge	insulation
CE, DH	2.375 mm	zero charge	insulation
EF, HG	2 mm	zero charge	insulation
FG	5 mm	zero charge	insulation
surface in ACDB		zero charge	initial value (10 mM)
surface in EFGH		zero charge	initial value (0 mM)



Supplementary Figure 12. Supplementary chemotactic capillary assay using the colony counting method for the condition of 0.2 mM indole in Supplementary Figure 9. **(a)** Agar plate pictures of colony counting after capillary assay. **(b)** Coefficient of variance calculated from the normalized counts.

Reference

(1) Ershov, D.; Phan, M.-S.; Pylvänäinen, J. W.; Rigaud, S. U.; Le Blanc, L.; Charles-Orszag, A.; Conway, J. R. W.; Laine, R. F.; Roy, N. H.; Bonazzi, D.; Duménil, G.; Jacquemet, G.; Tinevez, J.-Y. TrackMate 7: Integrating State-of-the-Art Segmentation Algorithms into Tracking Pipelines. *Nat Methods* **2022**, *19* (7), 829–832. https://doi.org/10.1038/s41592-022-01507-1

(2) Archit, A.; Freckmann, L.; Nair, S.; Khalid, N.; Hilt, P.; Rajashekar, V.; Freitag, M.; Teuber, C.; Spitzner, M.; Tapia Contreras, C.; Buckley, G.; Von Haaren, S.; Gupta, S.; Grade, M.; Wirth, M.; Schneider, G.; Dengel, A.; Ahmed, S.; Pape, C. Segment Anything for Microscopy. *Nat Methods* **2025**, *22* (3), 579–591. https://doi.org/10.1038/s41592-024-02580-4